

Unconventional p -wave and finite-momentum superconductivity induced by altermagnetism through the formation of Bogoliubov Fermi surface

SeungBeom Hong,¹ Moon Jip Park,^{1,2,*} and Kyoung-Min Kim^{3,†}

¹*Department of Physics, Hanyang University, Seoul 04763, Republic of Korea*

²*Research Institute for Natural Science, Hanyang University, Seoul 04763, Korea*

³*Center for Theoretical Physics of Complex Systems,
Institute for Basic Science, Daejeon 34126, Republic of Korea*

(Dated: July 3, 2024)

Altermagnet is an exotic class of magnetic materials wherein the Fermi surface exhibits a momentum-dependent spin-splitting while maintaining a net zero magnetization. Previous studies have shown that this distinctive spin-splitting can induce chiral p -wave superconductors or Fulde-Ferrell superconducting states carrying finite momentum. However, the underlying mechanisms of such unconventional superconductivities remain incompletely understood. Here, we propose that the formation of the Bogoliubov Fermi surface through the exchange field can play a significant role in such phenomena. Through a systematic self-consistent mean-field analysis on the extended attractive Hubbard model combined with the d -wave spin-splitting induced by the exchange field, as observed in RuO₂, we demonstrate that the formation of the Bogoliubov Fermi surface suppresses conventional spin-singlet superconducting states with s -wave characteristics. In contrast, the chiral p -wave state maintains a fully gapped spectrum without the Fermi surface, thereby becoming the ground state in the strong field regime. In the intermediate regime, we find that the Fulde-Ferrell state becomes the predominant state through the optimization of available channels for Cooper pairing. Moreover, we illustrate how the prevalence of the chiral p -wave and Fulde-Ferrell states over the s -wave state changes under the variation of the field strength or chemical potential. Our findings provide valuable insights into potential pathways for realizing sought-after topological p -wave superconductivity and finite momentum pairing facilitated by altermagnetism.

Introduction.— Breaking time-reversal symmetry (TRS) offers pathways to explore unconventional superconductivity beyond the conventional Bardeen–Cooper–Schrieffer (BCS) paradigm by inducing spin-split Fermi surfaces. While electrons encounter obstacles in forming spin-singlet Cooper pairs within the conventional framework [1], the spin-split Fermi surfaces may accommodate unconventional Cooper pairs with distinctive pairing symmetries. Noteworthy examples include p -wave topological superconductivity, which can be induced by external magnetic fields or within ferromagnetic metals, often implying the existence of intriguing Majorana edge or corner modes [2–4]. Alternatively, electrons can form finite-momentum pairings exhibiting nonuniform modulation in their pairing amplitudes, leading to the emergence of Fulde–Ferrell–Larkin–Ovchinnikov (FFLO) states [5–9].

Recently, considerable attention has been drawn to the impact of distinct TRS breaking patterns on superconductivity, stemming from a novel form of collinear magnetism known as altermagnetism [10–32]. In such systems, due to symmetry considerations, the Fermi surface displays momentum-dependent spin-splitting while maintaining a net magnetization of zero overall [33–37], contrasting with the spin-momentum locking typical of spin-orbit coupling. A prominent illustration of such an altermagnetic spin-splitting effect is the case of a two-dimensional altermagnetic metal like RuO₂, wherein the Fermi surface manifests d -wave-like spin splitting with a four-fold symmetric point nodal degeneracy. Remark-

ably, under applied strain, thin film RuO₂ exhibits superconductivity at relatively high temperatures, with $T_c = 1.7$ K [10], suggesting it as a promising platform for investigating the influence of such distinct spin-split Fermi surfaces on superconductivity. Previous theoretical studies have suggested intriguing phenomena related to superconductivity, including unconventional superconductivity [13, 14], Josephson effect [15–18], topological superconductivity with Majorana edge modes [19–21], orientation-dependent Andreev reflection [22, 23], finite-momentum Cooper pairing [24–27], gapless superconductivity [28], thermoelectric effect [29, 30], many body magnonic effect [31], and superconducting diode effect [32]. Despite significant recent advances, the impact of the altermagnetic spin-splitting effect on observed superconductivity in these systems remains incompletely understood.

In this Letter, we explore the emergence of unconventional superconducting states resulting from altermagnetic spin-splitting of the Fermi surface. Through a systematic mean-field analysis on the extended attractive Hubbard model [38] incorporating d -wave altermagnetic exchange fields, we uncover a spectrum of unconventional superconducting phenomena alongside conventional s -wave BCS states. Over a wide parameter range, we observe that the exchange fields suppress the s -wave BCS state by reducing the corresponding s -wave channel correlation function for Cooper pair formation, attributed to the formation of Bogoliubov Fermi surfaces (BFS) (Fig. 1(a)). Conversely, topological $p + ip$ super-

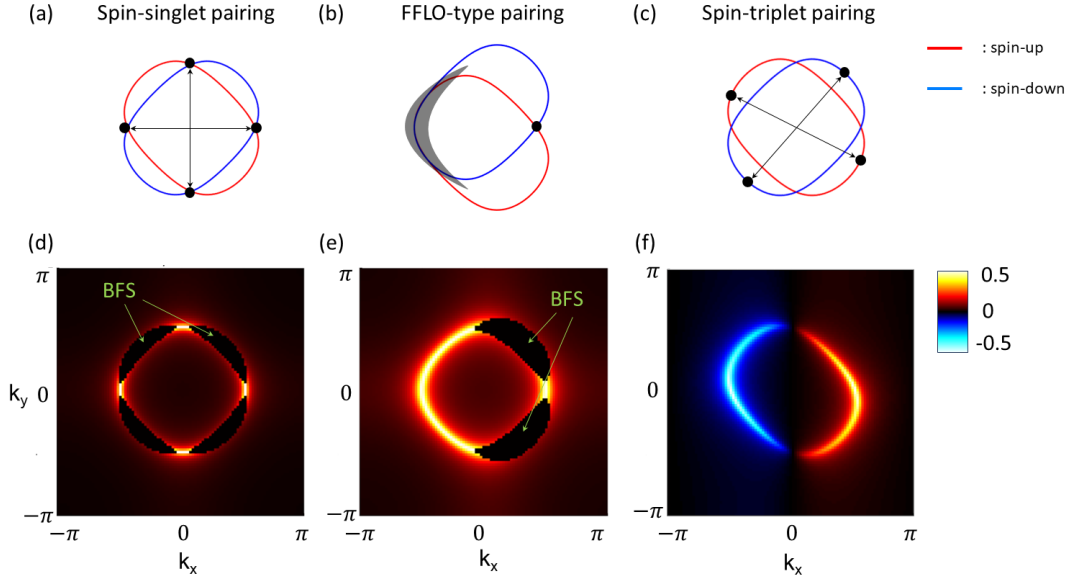


FIG. 1. The possible Fermi surface nesting scenarios under altermagnetic exchange field strength ($J/2t > 0.3$) are shown with (a) the singlet s -wave, (b) Fulde-Ferrell (FF), and (c) spin-triplet p -wave state, respectively. The red(blue) lines refers to the Fermi surface with spin-up(down) $\xi_{\pm\mathbf{k}} \pm J_{\pm\mathbf{k}} = 0$, especially $\xi_{\pm\mathbf{k}+\mathbf{q}} \pm J_{\pm\mathbf{k}+\mathbf{q}} = 0$ with the finite momentum \mathbf{q} in (b). The overlap of spin-up and down Fermi surface appears near four nodal points in (a), and near a single nodal line and single nodal point in (b), leading to the singlet pair nesting indicated by the gray region and black dots and arrows. On the other hand, as the Fermi surface overlaps with its inversion symmetric counterpart ($\mathbf{k} \rightarrow -\mathbf{k}$) over the entire Fermi surface, the triplet pairs can nest on the whole Fermi surface, indicated by the black dots and arrows. (d–f) The corresponding pair correlation functions are illustrated. The occurrence of Bogoliubov Fermi surface (BFS) in the singlet pairing causes the collapse of the pair correlation function to zero. However, in the spin-triplet pairing, there is no such collapse, sustaining the superconducting gap under the strong altermagnetic field limit.

conductivity is favored as the pertinent p -wave channel correlation function remains robust against the exchange field (Fig. 1(c)). Furthermore, we demonstrate that s -wave superconducting states with finite momentum pairing and accompanying BFS, namely ‘gapless FFLO states,’ may emerge as intermediate states preceding $p + ip$ states due to the augmentation of the available channels for Cooper pairing (Fig. 1(b)). These diverse manifestations highlight the symmetry-enriched unconventional superconductivity phenomena arising from the time-reversal symmetry breaking of altermagnetism.

Model.— We consider two-dimensional metallic systems possessing d -wave altermagnetism, as observed in RuO_2 [36, 37]. The model can be described using an effective tight-binding Hamiltonian given by

$$\hat{H} = \sum_{\mathbf{k}} c_{\mathbf{k}}^\dagger h_{\mathbf{k}} c_{\mathbf{k}} - U \sum_i n_{i\uparrow} n_{i\downarrow} - V \sum_{\sigma, \sigma'} \sum_{\langle i, j \rangle} n_{i\sigma} n_{j\sigma'}. \quad (1)$$

Here, $c_{\mathbf{k}}^\dagger = (c_{\mathbf{k}\uparrow}^\dagger, c_{\mathbf{k}\downarrow}^\dagger)$ is the creation operator of an electron with wave vector \mathbf{k} . $h_{\mathbf{k}} = \xi_{\mathbf{k}} I_2 + J_{\mathbf{k}} \sigma_z$ is the Bloch Hamiltonian. $\xi_{\mathbf{k}} = -2t(\cos(k_x) + \cos(k_y)) - \mu$, $J_{\mathbf{k}} = J \sin(k_x) \sin(k_y)$. t represents the hopping between nearest-neighbor sites, and μ is a chemical potential. $J_{\mathbf{k}}$ is the effective exchange field leading to d -wave-like spin splitting. The Bloch Hamiltonian, $h_{\mathbf{k}} = h(k_x, k_y)$, re-

spects $C_{4z}\mathcal{T}$ by satisfying $\sigma_y h^*(k_x, k_y) \sigma_y = h(k_y, -k_x)$. $n_{i\sigma} = c_{i\sigma}^\dagger c_{i\sigma}$ represents an electron density operator at i -site. In addition, the four nodal point degeneracy is protected despite the spin splitting in the Fermi surface (Fig. 1(a)). $U > 0$ and $V > 0$ represent the phonon-induced attractive onsite and nearest-neighbor density-density interactions, respectively. We explore a wide range of values for J , μ , and V : $0 \leq J/2t \leq 1$, $-2 \leq \mu/2t \leq 0$, and $0 \leq V/2t \leq 1.5$, while maintaining a fixed value of $U/2t = 1.5$. This allows us to investigate a range of superconducting orders across different scenarios.

To investigate the emergence of unconventional superconducting states, we conduct a self-consistent mean-field analysis utilizing the Bogoliubov-de-Gennes (BdG) formalism. Due to the presence of the inversion symmetry, the spin-singlet and triplet states remain uncoupled, allowing separate consideration. The following five distinct superconducting states may appear in our model [20, 38]: (i) s -wave spin-singlet (ii) Fulde-Ferrell (FF) spin-singlet state, originating from U , and the remaining three from V , which include (iii) extended s -wave spin-singlet, (iv) d -wave spin-singlet, (v) p -wave spin-triplet states. In the following, we focus on three predominant states: the s -wave state, the FF state, and the p -wave state. These states are prevalent within the parameter space under

consideration.

We utilize the following three pairing amplitudes:

$$\begin{aligned}\Delta_{\uparrow\downarrow}^s &= -\frac{U}{N} \sum_{\mathbf{k}} \langle c_{\mathbf{k}\uparrow} c_{-\mathbf{k}\downarrow} \rangle, \\ \Delta_{\uparrow\downarrow;\mathbf{q}}^{\text{FF}} &= -\frac{U}{N} \sum_{\mathbf{k}} \langle c_{\mathbf{k}+\mathbf{q}\uparrow} c_{-\mathbf{k}+\mathbf{q}\downarrow} \rangle, \\ \Delta_{\sigma\sigma}^{\text{p+ip}} &= -\frac{V}{N} \sum_{\mathbf{k}} (g_{\mathbf{k}}^{\text{p+ip}})^* \langle c_{\mathbf{k}\sigma} c_{-\mathbf{k}\sigma} \rangle,\end{aligned}\quad (2)$$

to characterize the s -wave ($\Delta_{\uparrow\downarrow}^s$), FF ($\Delta_{\uparrow\downarrow;\mathbf{q}}^{\text{FF}}$), and p -wave ($\Delta_{\sigma\sigma}^{\text{p+ip}}$) states. The FF state shares the s -wave characteristics of the s -wave state but features spatial modulation characterized by a finite wave vector \mathbf{q} . Here, $g_{\mathbf{k}}^{\text{p+ip}} = \sin(k_x) + i \sin(k_y)$ represents a square harmonics exhibiting $p_x + ip_y$ -like characteristics. As such, we refer to this p -wave state as a $p + ip$ state [20]. The BdG quasiparticle energy spectra of these states exhibit distinct gap-opening patterns, as shown by

$$\begin{aligned}E_{\mathbf{k}\sigma}^s &= \sqrt{\xi_{\mathbf{k}}^2 + |\Delta_{\uparrow\downarrow}^s|^2} + s(\sigma)J_{\mathbf{k}}, \\ E_{\mathbf{k}\sigma;\mathbf{q}}^{\text{FF}} &= \sqrt{\Xi_{\mathbf{k};\mathbf{q}}^2 + |\Delta_{\uparrow\downarrow;\mathbf{q}}^{\text{FF}}|^2} + s(\sigma)\Lambda_{\mathbf{k};\mathbf{q}}, \\ E_{\mathbf{k}\sigma}^{\text{p+ip}} &= \sqrt{(\xi_{\mathbf{k}} + s(\sigma)J_{\mathbf{k}})^2 + |\Delta_{\sigma\sigma}^{\text{p+ip}} g_{\mathbf{k}}^{\text{p+ip}}|^2},\end{aligned}\quad (3)$$

where $E_{\mathbf{k}\sigma}^s$ corresponds to the s -wave state, $E_{\mathbf{k}\sigma;\mathbf{q}}^{\text{FF}}$ to the FF state, and $E_{\mathbf{k}\sigma}^{\text{p+ip}}$ to the $p + ip$ state. The functions $\Xi_{\mathbf{k};\mathbf{q}} = \frac{1}{2}(\xi_{\mathbf{k}+\mathbf{q}} + J_{\mathbf{k}+\mathbf{q}} + \xi_{\mathbf{k}-\mathbf{q}} - J_{\mathbf{k}-\mathbf{q}})$ and $\Lambda_{\mathbf{k};\mathbf{q}} = \frac{1}{2}(\xi_{\mathbf{k}+\mathbf{q}} + J_{\mathbf{k}+\mathbf{q}} - \xi_{\mathbf{k}-\mathbf{q}} + J_{\mathbf{k}-\mathbf{q}})$ describe the modified dispersions for the FF phase with finite \mathbf{q} . We denote $s(\uparrow) = +1$ and $s(\downarrow) = -1$. The energies $E_{\mathbf{k}\sigma}^s$ and $E_{\mathbf{k}\sigma;\mathbf{q}}^{\text{FF}}$ may become negative under sufficient exchange field strength $J_{\mathbf{k}}$. In contrast, the gap $E_{\mathbf{k}\sigma}^{\text{p+ip}}$ of the $p + ip$ state maintains its gapped nature regardless of the field strength.

The pairing amplitudes, as presented in Eq. (2), are self-consistently determined solving the following gap equations:

$$\begin{aligned}\Delta_{\uparrow\downarrow}^s &= \frac{U}{N} \sum_{\mathbf{k}} \frac{\Delta_{\uparrow\downarrow}^s}{2\epsilon_{\mathbf{k}}^s} [1 - \Theta(-E_{\mathbf{k}\uparrow}^s) - \Theta(-E_{\mathbf{k}\downarrow}^s)], \\ \Delta_{\uparrow\downarrow;\mathbf{q}}^{\text{FF}} &= \frac{U}{N} \sum_{\mathbf{k}} \frac{\Delta_{\uparrow\downarrow;\mathbf{q}}^{\text{FF}}}{2\epsilon_{\mathbf{k};\mathbf{q}}^{\text{FF}}} [1 - \Theta(-E_{\mathbf{k}\uparrow;\mathbf{q}}^{\text{FF}}) - \Theta(-E_{\mathbf{k}\downarrow;\mathbf{q}}^{\text{FF}})], \\ \Delta_{\sigma\sigma}^{\text{p+ip}} &= \frac{V}{N} \sum_{\mathbf{k}} \frac{\Delta_{\sigma\sigma}^{\text{p+ip}} |g_{\mathbf{k}}^{\text{p+ip}}|^2}{2E_{\mathbf{k}\sigma}^{\text{p+ip}}}.\end{aligned}\quad (4)$$

In these equations, we denote $\epsilon_{\mathbf{k}}^s = \sqrt{\xi_{\mathbf{k}}^2 + |\Delta_{\uparrow\downarrow}^s|^2}$ and $\epsilon_{\mathbf{k};\mathbf{q}}^{\text{FF}} = \sqrt{\Xi_{\mathbf{k};\mathbf{q}}^2 + |\Delta_{\uparrow\downarrow;\mathbf{q}}^{\text{FF}}|^2}$. $\Theta(E)$ is the Heaviside step function. The gap equations for the s -wave and FF states incorporate form factors $[1 - \Theta(-E_{\mathbf{k}\uparrow}^s) - \Theta(-E_{\mathbf{k}\downarrow}^s)]$ and $[1 - \Theta(-E_{\mathbf{k}\uparrow;\mathbf{q}}^{\text{FF}}) - \Theta(-E_{\mathbf{k}\downarrow;\mathbf{q}}^{\text{FF}})]$, respectively. These factors exclude contributions from occupied BdG quasiparticle

states with negative energies ($E_{\mathbf{k}\sigma}^s < 0$ or $E_{\mathbf{k}\sigma;\mathbf{q}}^{\text{FF}} < 0$), reflecting the ground state's occupation of these states, which minimizes the system's energy. Conversely, $\Delta_{\sigma\sigma}^{\text{p+ip}}$ for the $p + ip$ state incorporates contributions from all BdG quasiparticle states.

The ground state energy for each state is calculated using the following energy expressions:

$$\begin{aligned}F_0^s &= \sum_{\mathbf{k}} \left[\xi_{\mathbf{k}} - \epsilon_{\mathbf{k}}^s + \frac{|\Delta_{\uparrow\downarrow}^s|^2}{U} \right] + \sum_{\mathbf{k},\sigma} \Theta(-E_{\mathbf{k}\sigma}^s) E_{\mathbf{k}\sigma}^s, \\ F_0^{\text{FF}}(\mathbf{q}) &= \sum_{\mathbf{k}} \left[\Xi_{\mathbf{k};\mathbf{q}} - \epsilon_{\mathbf{k};\mathbf{q}}^{\text{FF}} + \frac{|\Delta_{\uparrow\downarrow;\mathbf{q}}^{\text{FF}}|^2}{U} \right] \\ &\quad + \sum_{\mathbf{k},\sigma} \Theta(-E_{\mathbf{k}\sigma;\mathbf{q}}^{\text{FF}}) E_{\mathbf{k}\sigma;\mathbf{q}}^{\text{FF}}, \\ F_0^{\text{p+ip}} &= \frac{1}{2} \sum_{\mathbf{k},\sigma} \left[\xi_{\mathbf{k}} - E_{\mathbf{k}\sigma}^{\text{p+ip}} + \frac{|\Delta_{\sigma\sigma}^{\text{p+ip}}|^2}{V} \right],\end{aligned}\quad (5)$$

where F_0^s , $F_0^{\text{FF}}(\mathbf{q})$, and $F_0^{\text{p+ip}}$ correspond to the s -wave, FF, and $p + ip$ states, respectively. For the s -wave and FF states, the ground state energy incorporates contributions from the occupied BdG quasiparticle states with negative energy ($E_{\mathbf{k}\sigma}^s < 0$ or $E_{\mathbf{k}\sigma;\mathbf{q}}^{\text{FF}} < 0$) in addition to the usual energy contribution in the square brackets. In contrast, the ground state energy for the $p + ip$ state only contains the usual energy contribution due to its positive definite nature ($E_{\mathbf{k}\sigma}^{\text{p+ip}} > 0$). In the FF state, we identify the optimal \mathbf{q} vector by evaluating $F_0^{\text{FF}}(\mathbf{q})$ across various \mathbf{q} values and selecting the specific \mathbf{q} -value that yields the minimum of $F_0^{\text{FF}}(\mathbf{q})$ (refer to Fig. 3(a-b)). Refer to the Supplementary Material (SM) for the derivation of the gap equations and ground state energy expressions.

Results— We determine the favored superconducting states across a range of parameters $J/2t$, $V/2t$, and $\mu/2t$, by numerically solving the gap equations (Eq. (4)) and computing the ground state energy for each state (Eq. (5)). Fig. 2(a) plots the resulting phase diagram as a function of $J/2t$ and $V/2t$, showing three superconducting phases, the s -wave, FF, and $p + ip$ phases, each having the lowest energy in the respective region. We observe that the s -wave phase (the red region in Fig. 2(a)) predominates in the small exchange field regime ($J/2t \lesssim 0.28$). In this phase, the BdG quasiparticle energy spectra, $E_{\mathbf{k}\sigma}^s = \sqrt{\xi_{\mathbf{k}}^2 + |\Delta_{\uparrow\downarrow}^s|^2} + s(\sigma)J_{\mathbf{k}}$, exhibit a fully gapped structure in both spin sectors $\sigma = \uparrow, \downarrow$ (Fig. 2(c)). However, the exchange field $J_{\mathbf{k}}$ lifts their degeneracy, resulting in anisotropic, sign-alternating energy shifts (Fig. 2(d-e)). In $E_{\mathbf{k}\uparrow}^s$, the shifted energy $J_{\mathbf{k}}$ is negative along the line $k_x = -k_y$ or positive along $k_x = k_y$ (Fig. 2(d)). The magnitude of $J_{\mathbf{k}}$ reaches at its maximum value $J_* = J \sin^2(k_*)$, at $(k_x, k_y) = \pm(k_*, -k_*)$ where $k_* = \arccos\left(\frac{-(\mu-J)}{2t + \sqrt{(2t)^2 - J(\mu-J)}}\right)$. At this point,

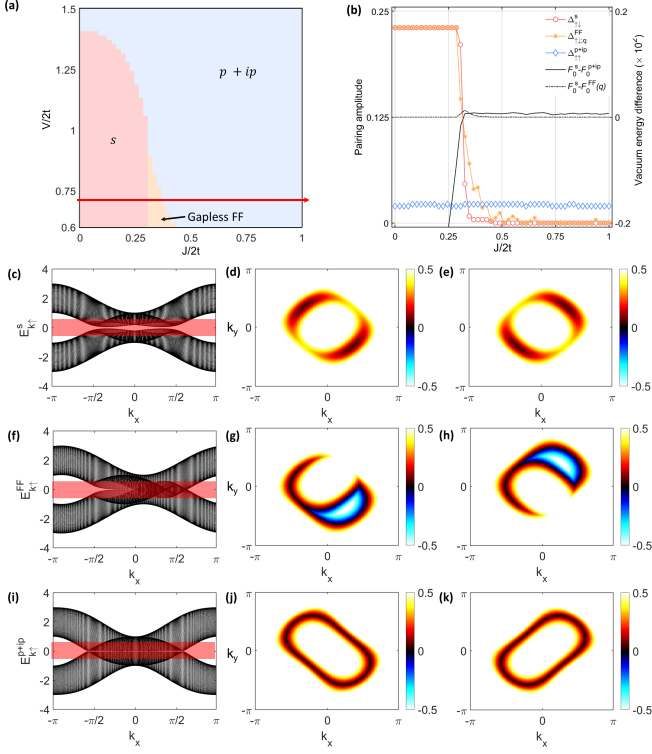


FIG. 2. (a) Phase diagram illustrates three superconducting phases: s -wave phase (denoted by ‘ s ’), FF phase (‘gapless FF’), and $p + ip$ phase (‘ $p + ip$ ’) with the fixed $U/2t = 1.5$, $\mu/2t = -1$. (b) Evolution of the pairing amplitude (left axis) and vacuum energy difference (right axis) in each superconducting state as a function of $J/2t$. Here, $(\Delta_{\uparrow\downarrow}^s, F_0^s)$ correspond to the s -wave state, $(\Delta_{\uparrow\downarrow;q}^{FF}, F_0^{FF}(\mathbf{q}))$ correspond to the FF state, and $(\Delta_{\uparrow\uparrow}^{p+ip}, F_0^{p+ip})$ correspond to the $p + ip$ state. The value of $V/2t = 0.7$ is fixed, while the value of $J/2t$ is varied, as indicated by the red arrow in (a). Energy spectra of Bogoliubov-de-Gennes (BdG) quasiparticles (c–e) $E_{\mathbf{k}\sigma}^s$ in the s -wave state with $J/2t = 0.2$, (f–h) $E_{\mathbf{k}\sigma;q}^{FF}$ in the FF state with $J/2t = 0.3$, and (i–k) $E_{\mathbf{k}\sigma}^{p+ip}$ in the $p + ip$ state with $J/2t = 0.8$ are shown. In (c, f, i), each energy spectrum is displayed in the range of $k_x \in [-\pi, \pi]$. Different curves indicate distinct values of k_y from $-\pi$ to π . In (d–e, g–h, j–k), energy spectrum for $\sigma = \uparrow, \downarrow$ within the red-marked window in (c, f, i), respectively are displayed through the color scale across (k_x, k_y) . The region scaled with blue shows the BFS in quasiparticle spectrum.

$J_{\mathbf{k}}$ effectively reduces the energy gap as $\Delta_{\uparrow\downarrow}^s - J_*$, which aligns with the actual gap size $\bar{\Delta}_{\text{band}}$ in the energy spectra (e.g., $\Delta_{\uparrow\downarrow}^s = 0.2296$, $J_* = 0.1355$, and $\bar{\Delta}_{\text{band}} = 0.0789 \approx \Delta_{\uparrow\downarrow}^s - J_*$ for the energy spectra presented in Fig. 2(c)). It is important to note that as long as J_* does not exceed $\Delta_{\uparrow\downarrow}^s$, $E_{\mathbf{k}\sigma}^s$ can maintain their full gap structures, ensuring that the s -wave state remains the ground state of the system. The opposite pattern is observed in $E_{\mathbf{k}\sigma}^s$ (Fig. 2(e)).

As J further increases to $J/2t = 0.28$, J_* starts to exceed $\Delta_{\uparrow\downarrow}^s$, leading to the gap closing and the formation

of BFS in $E_{\mathbf{k}\sigma}^s < 0$ in the s -wave state. We note that the formation of the BFS indicates the exclusion of contributions from these occupied BdG quasiparticle states in the self-consistency relation of $\Delta_{\uparrow\downarrow}^s$ (refer to the corresponding gap equation in Eq. (4)). Consequently, $\Delta_{\uparrow\downarrow}^s$ is significantly suppressed, leading to a considerable increase in the energy of the s -wave state (Fig. 2(b)). Hence, the s -wave state is disfavored in this regime. Alternatively, the FF state becomes the most energetically favored state in this regime (the orange region in Fig. 2(a)), which possesses a more pronounced pairing amplitude and reduced energy compared to the s -wave state (Fig. 2(b)). The BdG quasiparticle energy spectra of the FF state, $E_{\mathbf{k}\sigma;q}^{FF} = \sqrt{\Xi_{\mathbf{k};q}^2 + |\Delta_{\uparrow\downarrow;q}^{FF}|^2} + s(\sigma)\Lambda_{\mathbf{k};q}$, exhibit the formation of BFS in both spin sectors $\sigma = \uparrow, \downarrow$ (Fig. 2(f)) with anisotropic, sign-alternating energy shifts due to the modified exchange field $\Lambda_{\mathbf{k};q}$ (Fig. 2(g–h)), similar to the s -wave state (Fig. 2(d–e)). However, in contrast to the s -wave state, the finite momentum pairing through $\Delta_{\uparrow\downarrow;q}^{FF}$ results in the distorted pattern breaking the reflection symmetry across the line $k_x = -k_y$ or $k_x = k_y$ in the energy spectra.

One plausible explanation for the dominance of the FF state over the s -wave state is the broader overlap between the dispersions of spin-up electrons ($\xi_{\mathbf{k}+\mathbf{q}} + J_{\mathbf{k}+\mathbf{q}}$) and spin-down holes ($-\xi_{-\mathbf{k}+\mathbf{q}} + J_{-\mathbf{k}+\mathbf{q}}$), pivotal for finite momentum pairing $c_{\mathbf{k}+\mathbf{q}\uparrow}c_{-\mathbf{k}+\mathbf{q}\downarrow}$ (the marked region in Fig. 1(b)). Within this overlapped region, the ‘energy cost’ stemming from the modified dispersion diminishes due to the overlap (i.e., $\Xi_{\mathbf{k};q} = \frac{1}{2}(\xi_{\mathbf{k}+\mathbf{q}} + J_{\mathbf{k}+\mathbf{q}} + \xi_{\mathbf{k}-\mathbf{q}} - J_{\mathbf{k}-\mathbf{q}}) \approx 0$) (see the corresponding equation in Eq. (4)). This extended overlap enhances the contribution to the FF state’s pairing amplitude $\Delta_{\uparrow\downarrow;q}^{FF}$, resulting in an increased value of $\Delta_{\uparrow\downarrow;q}^{FF}$ despite the presence of the BFS. In this scenario, the specific \mathbf{q} vector characterizing the FF state is determined by optimizing available channels for Cooper pairing. Our analysis reveals that there are four possibilities for the direction of \mathbf{q} : $\pm\hat{x}$ and $\pm\hat{y}$, all of which exhibit degenerate energy levels (Fig. 3(b)). It is noteworthy that these \mathbf{q} vectors align with the hopping directions, pointing along one of the lattice vector directions such as $\pm\hat{x}$ and $\pm\hat{y}$. Furthermore, our study shows a rising trend in the magnitude of the \mathbf{q} vector as the exchange field $J_{\mathbf{k}}$ increases (Fig. 3(c)).

The $C_{4z}\mathcal{T}$ symmetry inherent in the model indicates the presence of four-fold degenerate ground state manifolds, characterized by $\mathbf{q} = \pm(q_0, 0), \pm(0, q_0)$. In our investigation, we choose one configuration among these four possibilities. However, in principle, one can compose various linear superpositions of the four FF states with different \mathbf{q} , which possibly have lower energy states. Among these compositions, the only possible superconducting order parameter which preserves $C_{4z}\mathcal{T}$ is multiple \mathbf{q} -state, which is given as $\Delta \sim \Delta_{(+q_0, 0)} + \Delta_{(-q_0, 0)} + \Delta_{(0, +q_0)} + \Delta_{(0, -q_0)}$. While the single- \mathbf{q} FF state pre-

serves the effective translational symmetry with the gauge transformation, the multiple- q FF state gives rise to a pair-density wave that breaks the translational symmetry. The investigations on the finer energetic splitting can elucidate the energy differentials between these pair-density waves [39].

We emphasize the unusual occurrence of the observed gapless FF state in our study, distinguishing it from instances of gapless superconductivity [28] and the FF state [24–27] separately reported in previous studies. It is also worth mentioning that the observed s -wave FF state is different from the d -wave FF state reported in Ref. [24] due to the difference in the chemical potential.

Upon entering the strong field regime ($J/2t \gg 0.28$), we observe the formation of the $p + ip$ phase (the blue region in Fig. 2(a)). In this phase, the BdG quasiparticle energy spectra, $E_{\mathbf{k}\sigma}^{p+ip} = \sqrt{(\xi_{\mathbf{k}} + s(\sigma)J_{\mathbf{k}})^2 + |\Delta_{\sigma\sigma}^{p+ip}g_{\mathbf{k}}^{p+ip}|^2}$, maintain a fully gapped structure (Fig. 2(i)), regardless of the field strength; except for the case $\mu/2t = 0$, where the energy spectra possess nodal points at $(k_x, k_y) = (\pi, 0), (0, \pi)$. The preserved gap structure ensures a significant pairing amplitude $\Delta_{\sigma\sigma}^{p+ip}$ (Fig. 2(i)), as most of the BdG quasiparticle states contribute to $\Delta_{\sigma\sigma}^{p+ip}$ in contrast to the s -wave and FF states (see Eq. (4)). Consequently, effective energy minimization is achieved through the gap opening throughout the entire normal-state Fermi surface, establishing the $p + ip$ phase as a stable phase in the strong field regime. The influence of the exchange field primarily results in anisotropic energy spectra without the formation of the BFS (Fig. 2(j–k)).

We attribute the emergence of the $p + ip$ phase in the strong field regime ($J/2t \gg 1$) to its persistent pair correlation function, $(g_{\mathbf{k}}^{p+ip})^* \langle c_{\mathbf{k}\sigma} c_{-\mathbf{k}\sigma} \rangle$. In the $p + ip$ phase, the absence of BFS leads to the preservation of the pair correlation function across most of the normal-state Fermi surface, excluding at nodal points where the corresponding square harmonics $g_{\mathbf{k}}^{p+ip}$ vanishes (Fig. 1(f)). This stands in contrast with the pair correlation function of the s -wave state, $\langle c_{\mathbf{k}\uparrow} c_{-\mathbf{k}\downarrow} \rangle$, which excludes contributions from occupied BdG quasiparticle states, pertaining only four nodal points where the exchange field vanishes (Fig. 1(d)). With increasing field strength, the presence of occupied BdG quasiparticle states becomes more pronounced. Therefore, in the strong field regime, the $p + ip$ phase emerges as the most energetically favored state due to the amplified exclusion of contributions from these states to the pairing amplitude.

The stabilization of the $p + ip$ state over conventional BCS states indicates a promising avenue toward the realization of topological chiral superconductivity. Due to the degeneracy between $p + ip$ and $p - ip$ states, there exist two distinct pairing symmetries. The $p + ip$ state, characterized by equal chirality of both spin sectors, exhibits a net Chern number $|C| = 2$, resulting in the appearance

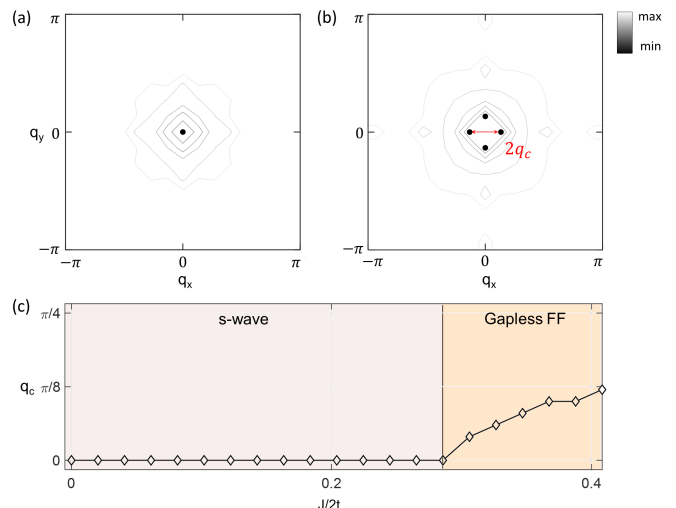


FIG. 3. (a–b) Energy landscape of the the FF state vacuum energy $F_0^{FF}(\mathbf{q})$ as a function of the pairing momentum vector $\mathbf{q} = (q_x, q_y)$. The minimum energy points are marked by the black dots. (c) Evolution of the optimal pairing momentum \mathbf{q}_c that minimizes the vacuum energy. $J/2t = 0.2$ and $J/2t = 0.3$ are utilized in (a) and (b), respectively. In all panels, The parameters $V/2t = 0.7$, $U/2t = 1.5$, and $\mu/2t = -1$ are utilized.

of symmetry-protected chiral edge modes [20]. There is another spin-triplet state of the $p + ip$ type, known as the ‘helical p -wave state,’ which can be stabilized. This state exhibits opposite chiralities between spin-up and spin-down sectors and possesses a vanishing Chern number $C = 0$, indicating an adiabatic connection to the topologically trivial superconductor. It is worth noting that although the degeneracy exists between the chiral states within our model, the presence of weak $C_{4z}\mathcal{T}$ -breaking Rashba spin-orbit coupling energetically favors the helical state over the chiral state [20].

It is worth mentioning that while we primarily focus on the s -wave, FF, and $p + ip$ states out of the five potential superconducting states considered in this study, the other two states—the extended s -wave and d -wave states—may emerge when $V/2t$ is sufficiently large. This behavior aligns with previous studies on the extended Hubbard model for cuprates [40]. Moreover, our investigation reveals that these states can become prevalent when the exchange field is small ($J/2t \ll 1$) and the chemical potential μ is tuned to $\mu/2t = -2$ or $\mu/2t = 0$. For additional details about our analysis, refer to the SM.

Discussion.— Our investigation into the unconventional superconductivity of two-dimensional altermagnetic metals has uncovered intriguing possibilities beyond conventional BCS states. Through rigorous theoretical analysis, we have elucidated the emergence of topological $p \pm ip$ states, BFSs, and FFLO phase triggered by the interplay between exchange interactions and nearest-

neighbor attractive interactions. The occurrence of the BFS plays a crucial role in significantly suppressing conventional BCS superconductivity, thereby enabling the realization of these alternative unconventional superconducting states. Particularly noteworthy is the observation that $p \pm ip$ superconductivity can be stabilized with relatively small nearest-neighbor interaction strengths compared to onsite interactions. This phenomenon offers a promising avenue towards the realization of topological chiral superconductivity.

We note that further experiments, such as the London penetration depth measurement, can reveal information about the superconducting gap structure. d -wave exchange field of altermagnetism may induce the ‘nodal-like’ signature for the BCS state characterized by linear T -dependence of the penetration depth, while p -wave superconductivity shows a rather fully gapped structure. This feature is different from commonly observed phenomena of conventional metallic superconductors. The observed superconductivity in RuO_2 occurs in the presence of strain that explicitly breaks the underlying $C_{4z}\mathcal{T}$ symmetry. While the four-fold symmetric ground state manifold of the FFLO instability is reminiscent of the original rotational symmetry, the application of the strain would lift the ground state manifold, which would allow the strain engineering of the superconducting pairing symmetry. The study on the effect of the external rotational-symmetry breaking strain would be an interesting topic for future study.

ACKNOWLEDGEMENT

M.J.P. thanks Changyoung Kim and Gibaik Sim for the fruitful discussions. This work was supported by the National Research Foundation of Korea (NRF) grant funded by the Korea government (MSIT) (Grants No. RS-2023-00252085 and No. RS-2023-00218998). K.-M.K. was supported by the Institute for Basic Science in the Republic of Korea through the project IBS-R024-D1.

* moonjippark@hanyang.ac.kr

† kmkim@ibs.re.kr

- [1] M. Sigrist and K. Ueda, Phenomenological theory of unconventional superconductivity, *Rev. Mod. Phys.* **63**, 239 (1991).
- [2] X.-L. Qi and S.-C. Zhang, Topological insulators and superconductors, *Rev. Mod. Phys.* **83**, 1057 (2011).
- [3] M. Sato and Y. Ando, Topological superconductors: a review, *Rep. Prog. Phys.* **80**, 076501 (2017).
- [4] M. Sato and S. Fujimoto, Majorana fermions and topology in superconductors, *J. Phys. Soc. Jpn.* **85**, 072001 (2016).
- [5] J. Wosnitzer, Fflo states in layered organic superconductors, *Annalen der Physik* **530**, 1700282 (2018), <https://onlinelibrary.wiley.com/doi/pdf/10.1002/andp.201700282>.
- [6] Y. Matsuda and H. Shimahara, Fulde-ferrell-larkin-ovchinnikov state in heavy fermion superconductors, *Journal of the Physical Society of Japan* **76**, 051005 (2007), <https://doi.org/10.1143/JPSJ.76.051005>.
- [7] K. Michaeli, A. C. Potter, and P. A. Lee, Superconducting and ferromagnetic phases in $\text{SrTiO}_3/\text{LaAlO}_3$ oxide interface structures: Possibility of finite momentum pairing, *Phys. Rev. Lett.* **108**, 117003 (2012).
- [8] N. F. Q. Yuan and L. Fu, Topological metals and finite-momentum superconductors, *Proc. Natl. Acad. Sci. U.S.A.* **118**, e2019063118 (2021).
- [9] A. Q. Chen, M. J. Park, S. T. Gill, Y. Xiao, D. Reig-i Plessis, G. J. MacDougall, M. J. Gilbert, and N. Mason, Finite momentum cooper pairing in three-dimensional topological insulator josephson junctions, *Nature Communications* **9**, 3478 (2018).
- [10] M. Uchida, T. Nomoto, M. Musashi, R. Arita, and M. Kawasaki, Superconductivity in uniquely strained RuO_2 films, *Phys. Rev. Lett.* **125**, 147001 (2020).
- [11] H. G. Gil and J. Linder, Superconductor-altermagnet memory functionality without stray fields (2024), [arXiv:2308.10939 \[cond-mat.supr-con\]](https://arxiv.org/abs/2308.10939).
- [12] B. Brekke, A. Brataas, and A. Sudbø, Two-dimensional altermagnets: Superconductivity in a minimal microscopic model, *Phys. Rev. B* **108**, 224421 (2023).
- [13] A. Bose, S. Vadnais, and A. Paramakanti, *Altermagnetism and superconductivity in a multiorbital t-j model* (2024), [arXiv:2403.17050 \[cond-mat.str-el\]](https://arxiv.org/abs/2403.17050).
- [14] B. Brekke, A. Brataas, and A. Sudbø, Two-dimensional altermagnets: Superconductivity in a minimal microscopic model, *Physical Review B* **108**, 10.1103/physrevb.108.224421 (2023).
- [15] J. A. Ouassou, A. Brataas, and J. Linder, dc josephson effect in altermagnets, *Physical Review Letters* **131**, 10.1103/physrevlett.131.076003 (2023).
- [16] J.-X. Hu, O. Matsyshyn, and J. C. W. Song, *Non-linear superconducting magnetoelectric effect* (2024), [arXiv:2404.18616 \[cond-mat.supr-con\]](https://arxiv.org/abs/2404.18616).
- [17] Q. Cheng and Q.-F. Sun, Orientation-dependent josephson effect in spin-singlet superconductor/altermagnet/spin-triplet superconductor junctions, *Physical Review B* **109**, 10.1103/physrevb.109.024517 (2024).
- [18] H. G. Gil and J. Linder, Superconductor-altermagnet memory functionality without stray fields, *Physical Review B* **109**, 10.1103/physrevb.109.134511 (2024).
- [19] Y.-X. Li and C.-C. Liu, Majorana corner modes and tunable patterns in an altermagnet heterostructure, *Physical Review B* **108**, 10.1103/physrevb.108.205410 (2023).
- [20] D. Zhu, Z.-Y. Zhuang, Z. Wu, and Z. Yan, Topological superconductivity in two-dimensional altermagnetic metals, *Phys. Rev. B* **108**, 184505 (2023).
- [21] S. A. A. Ghorashi, T. L. Hughes, and J. Cano, Altermagnetic routes to majorana modes in zero net magnetization (2023), [arXiv:2306.09413 \[cond-mat.mes-hall\]](https://arxiv.org/abs/2306.09413).
- [22] M. Papaj, Andreev reflection at the altermagnet-superconductor interface, *Physical Review B* **108**, 10.1103/physrevb.108.1060508 (2023).
- [23] C. Sun, A. Brataas, and J. Linder, *Andreev reflection in altermagnets* (2023), [arXiv:2303.14236 \[cond-mat.supr-con\]](https://arxiv.org/abs/2303.14236).

- con].
- [24] D. Chakraborty and A. M. Black-Schaffer, Zero-field finite-momentum and field-induced superconductivity in altermagnets (2023), [arXiv:2309.14427 \[cond-mat.supr-con\]](#).
- [25] S.-B. Zhang, L.-H. Hu, and T. Neupert, Finite-momentum cooper pairing in proximitized altermagnets, *Nat. Commun.* **15**, 1801 (2024).
- [26] H. G. Giil, B. Brekke, J. Linder, and A. Brataas, Quasiclassical theory of superconducting spin-splitter effects and spin-filtering via altermagnets (2024), [arXiv:2403.04851 \[cond-mat.supr-con\]](#).
- [27] A. A. Zyuzin, Magnetolectric effect in superconductors with d-wave magnetization (2024), [arXiv:2402.15459 \[cond-mat.supr-con\]](#).
- [28] M. Wei, L. Xiang, F. Xu, L. Zhang, G. Tang, and J. Wang, Gapless superconducting state and mirage gap in altermagnets (2023), [arXiv:2308.00248 \[cond-mat.supr-con\]](#).
- [29] P. O. Sukhachov, E. W. Hodt, and J. Linder, Thermoelectric effect in altermagnet-superconductor junctions (2024), [arXiv:2404.10038 \[cond-mat.supr-con\]](#).
- [30] S. Chourasia, A. Svetogorov, A. Kamra, and W. Belzig, Thermodynamic properties of a superconductor interfaced with an altermagnet (2024), [arXiv:2403.10456 \[cond-mat.supr-con\]](#).
- [31] K. Mæland, B. Brekke, and A. Sudbø, Many-body effects on superconductivity mediated by double-magnon processes in altermagnets, *Physical Review B* **109**, 10.1103/physrevb.109.134515 (2024).
- [32] S. Banerjee and M. S. Scheurer, Altermagnetic superconducting diode effect (2024), [arXiv:2402.14071 \[cond-mat.supr-con\]](#).
- [33] I. I. Mazin, Altermagnetism in mnTe: Origin, predicted manifestations, and routes to detwinning, *Phys. Rev. B* **107**, L100418 (2023).
- [34] S. Lee, S. Lee, S. Jung, J. Jung, D. Kim, Y. Lee, B. Seok, J. Kim, B. G. Park, L. Šmejkal, C.-J. Kang, and C. Kim, Broken kramers degeneracy in altermagnetic mnTe, *Phys. Rev. Lett.* **132**, 036702 (2024).
- [35] S. Reimers, L. Odenbreit, L. Šmejkal, V. N. Strocov, P. Constantinou, A. B. Hellenes, R. Jaeschke Ubiergo, W. H. Campos, V. K. Bharadwaj, A. Chakraborty, T. Denneulin, W. Shi, R. E. Dunin-Borkowski, S. Das, M. Kläui, J. Sinova, and M. Jourdan, Direct observation of altermagnetic band splitting in crsb thin films, *Nature Communications* **15**, 10.1038/s41467-024-46476-5 (2024).
- [36] K.-H. Ahn, A. Hariki, K.-W. Lee, and J. Kuneš, Antiferromagnetism in ruo₂ as *d*-wave pomeranchuk instability, *Phys. Rev. B* **99**, 184432 (2019).
- [37] L. Šmejkal, R. González-Hernández, T. Jungwirth, and J. Sinova, Crystal time-reversal symmetry breaking and spontaneous hall effect in collinear antiferromagnets, *Science Advances* **6**, eaaz8809 (2020), <https://www.science.org/doi/pdf/10.1126/sciadv.aaz8809>.
- [38] W.-C. Chen, Y. Wang, and C.-C. Chen, Superconducting phases of the square-lattice extended hubbard model, *Phys. Rev. B* **108**, 064514 (2023).
- [39] G. Sim and J. Knolle, In preparation (2024).
- [40] R. Micnas, J. Ranninger, S. Robaszkiewicz, and S. Tabor, Superconductivity in a narrow-band system with intersite electron pairing in two dimensions: A mean-field study, *Phys. Rev. B* **37**, 9410 (1988).